JOURNAL OF SOLID STATE CHEMISTRY 62, 112–132 (1986)

High-Resolution Transmission Electron Microscopy and X-Ray Microanalysis of Chemical Reactions in the Gold–Tin Thin-Film System

D. C. DUFNER* AND L. EYRING†

Department of Chemistry and the Center for Solid State Science, Arizona State University, Tempe, Arizona 85287

Received January 28, 1985; in revised form September 16, 1985

The gold–tin system is widely studied. Several models for the interdiffusion process, leading to the formation of the gold–tin phases, have been published in the literature. To clarify some of these reaction mechanisms, observations in the thin-film specimens have been made by the use of high-resolution transmission electron microscopy (HREM) and X-ray microanalysis. Thin-film specimens have been prepared by depositing individual thin films of gold and tin and combining them into a two-film arrangement. In addition, gold has been evaporated directly onto a thin tin film. Reactions at room temperature were not found in the two-film couples, but after heating at 200°C for 10 min, several expected and unexpected reactions were observed. The rate of reaction of the gold-islands-on-tin-films arrangement depended on the freshness of the tin film. The cause of the initial lack of reaction was determined to be due to the presence of an intervening amorphous contamination layer between the gold and tin films, which acts as a diffusion barrier. An $AuSn_2$ phase, possibly metastable, having a structure different from that of the equilibrium $AuSn_2$ phase, was studied in detail. Electron diffraction patterns were frequently observed from unknown phases. Possible models for the formation of the new phases are suggested. The contamination layers in the two-film couples effectively control the rate and extent of the gold–tin reactions.

Introduction

The general goal of this research is to clarify mechanisms of solid state reactions at the atomic level as a step in the rationalization of macroscopic reaction behavior in solids. A study of chemical reactions occurring as interdiffusion or other transport processes proceed in thin films can be made by means of high-resolution transmission electron microscopy (HREM). The chemistry of the near-surface region represents a vital, but not yet well-understood regime. In this research, chemical changes occurring near interfaces in solid specimens which are very thin (< 200 Å) in at least one direction are studied. These specimens are prepared in most cases by vacuum evaporation as well as by the usual methods of thinning bulk materials. The structures existing both in the original preparation and as subsequently modified by heating or changed by the conditions in the microscope are examined and compared. Differences in chemical behavior between thin films and the thinned bulk material are to be explored.

* Current address: Pennzoil Company, Technology Division, P.O. Box 7569, The Woodlands, Tex. 77387.

† To whom correspondence should be addressed.

0022-4596/86 $3.00

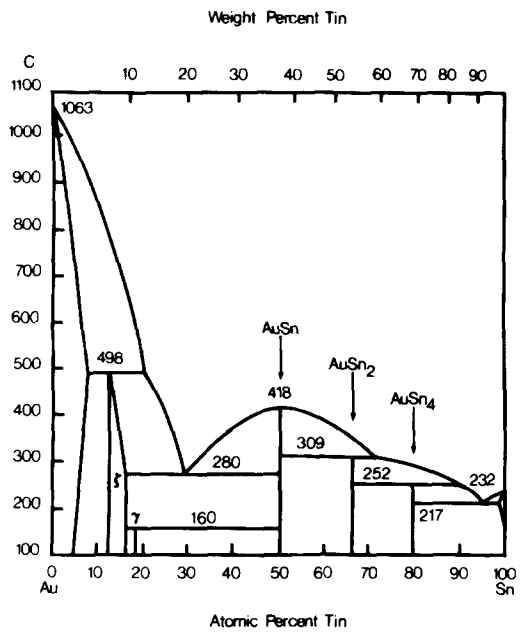

FIG. 1. The gold–tin phase diagram.

HREM is ideally suited for this type of study since it is capable of revealing localized atomic structures near interfaces. The extrapolation from atomic to bulk properties can thereby be advanced.

The widely studied gold–tin system has been chosen for this study. The phase diagram, shown in Fig. 1, has remained essentially unchanged since the original work by Vogel (*1*). The crystal data for the established gold–tin phases are listed in Table 1.

Gold and tin form a very fast diffusion system (*20*). The interdiffusion of gold and tin at room temperature can result in the formation of the gold–tin phases. Studies, based on transmission electron microscopy, X-ray diffraction, and Rutherford backscattering techniques (*21–32*), have revealed a number of metallurgical phenomena involving bulk and grain boundary diffusion mechanisms and intermetallic compound formation.

One of the earliest works involving interdiffusion of gold and tin was published by Tu and Rosenberg (*32*). They performed X-ray diffraction studies on various bimetallic thin-film couples and found that these couples readily interdiffuse at room temperature and also form intermetallic compounds. By using various thickness combinations in thin film couples, Buene (*20*), Simić and Marinković (*31*), and Nakahara and McCoy

TABLE I

CRYSTAL DATA FOR THE GOLD–TIN PHASES

Phase	Composition (at % Sn)	Structure	Space group	Z	Dimensions (Å)	Reference
Au	0.0	f.c.c.	$Fm3m$	4	a = 4.0786	*2*
Sn	100.0	b.c.t.	$I4_1/amd$	4	a = 5.831	*3*
					c = 3.182	
Zeta (ζ)	12.0–16.0	h.c.p.			a = 2.92	*4–8*
					c = 4.78	
Au_5Sn (γ)	16.0	Hexagonal	$R3$	3	a = 5.05	*9*
					c = 14.34	
AuSn (δ)	50.0	Hexagonal	$P6_3mmc$	2	a = 4.323	*10–15, 19*
					c = 5.517	
$AuSn_2$ (ε)	66.7	Orthorhombic	$Pbca$	8	a = 6.908	*4, 14, 16, 17*
					b = 7.037	
					c = 11.788	
$AuSn_4$ (η)	80.0	Orthorhombic	$Aba2$	4	a = 6.446	*14, 18*
					b = 6.484	
					c = 11.599	

(*29*) have found the intermetallic phases AuSn, $AuSn_2$, $AuSn_4$, and ζ to be formed by room temperature interdiffusion.

Buene *et al.* (*25*) have studied the time development of the gold–tin phases by TEM. The results suggest that both AuSn and $AuSn_4$ are nucleated at the beginning of the interdiffusion. The $AuSn_4$ phase disappears together with tin in the presence of excess gold, whereas the AuSn phase disappears together with gold in the presence of excess tin. The appearance of $AuSn_2$ results from the transformation of AuSn. The transformation of $AuSn_2$ into $AuSn_4$ is found to take place very slowly, which is consistent with the earlier RBS results (*21*, *22*).

One of the more interesting questions in the understanding of thin-film interdiffusion is which intermetallic phase will be formed first. As just mentioned, two phases, AuSn and $AuSn_4$, have been known to form within a few minutes or hours after deposition (*25*). The formation of $AuSn_4$ as a first phase can be justified by the structural relationship between β-tin and $AuSn_4$, described by Buene (*25*). The rapid diffusion of gold atoms into tin permits the nucleation of $AuSn_4$ without drastically changing the β-tin structure.

Why AuSn forms as a first phase is not clear at this time (*30*). The understanding of a structural relationship between AuSn and tin is of considerable interest in attempting to answer this question. AuSn possesses a nickel arsenide (NiAs) structure, in which the gold atoms occupy the octahedral holes in an h.c.p. array of tin atoms. The NiAs structure provides a convenient model for further transformation, as AuSn can transform into a gold- or a tin-richer phase (Raynor (*33*)). Also, since NiAs is hexagonal, the transformation can also proceed by the adjustment of the *c*/*a* ratio.

The proposed reaction mechanisms have been found to be affected by the presence of impurities in the thin films. If tin is oxidized before the evaporation of gold, a surface oxide, SnO_2, is formed and acts as a diffusion barrier (*21*). Other barriers can be due to the condensation of residual vapors and impurities on the tin film before the evaporation of gold (*27*).

In spite of the wealth of information provided by the interdiffusion studies, there is an absence of HREM observations of the gold–tin reactions. The purpose of this research is to use HREM and X-ray microanalysis to study the structural and compositional changes occurring in the thin-film gold–tin system in order to elucidate the mechanisms by which the gold–tin phases are formed.

Experimental

The preparation of the gold and tin thin films is accomplished by vacuum deposition in high vacuum. The high-vacuum vapor deposition apparatus consists of two refractory metal evaporation sources, a substrate holder/heater assembly, and a thin-film thickness and rate monitor (Infincon Model XTM, Infincon Leybold-Heraeus, Inc.) mounted inside a standard 32-cm-diam glass bell jar. The vacuum is provided by a combination of two Sargent-Welch Model 1402 roughing pumps and a CVC 4-in. Blueline oil diffusion pump filled with Santovac-5 diffusion pump oil and equipped with a liquid nitrogen-cooled chevron baffle trap. Base pressures of $\sim 6 \times 10^{-7}$ Torr can be achieved by pumping for a period of 1.5 to 2 hr.

The thickness monitor is used to record film thicknesses and to monitor the rate of deposition. It is capable of recording thicknesses to 1 Å at rates as low as 0.1 Å/sec with less than 2% error. Measurements are made with a quartz crystal oscillator mounted in a water-cooled sensor, which is placed approximately 40 cm above the evaporation sources, next to the substrate

holder/heater assembly. Variable transformers are used in conjunction with the thickness monitor by regulating the amount of current passing through the evaporation filaments so as to achieve the desired deposition rate.

A central item in the evaporator system is the substrate holder/heater assembly. The design for the substrate heater was taken from Naber (*34*), the scale in this case being one-half that described. Electron bombardment heats a 0.7-mm-thick tungsten sheet, which is in thermal contact with a 1.5-mm-thick tantalum substrate holder plate mounted above a water-cooled stainless steel base. A silicon controlled rectifier temperature controller (Eurotherm Corp., Models 919 and 931) automatically controls the temperature by regulating the emission current of the thoriated tungsten filaments (General Electric Co.). The temperature is monitored by a Pt/Pt-10%Rh thermocouple mounted in the substrate holder plate and connected to the temperature set-point unit, a digital thermometer (Omega Engineering, Inc., Model 2160A), and a strip chart recorder (Omega Model 285) for long-term temperature monitoring. Power to the filaments is provided by a 3 kV, 330 mA D.C. power supply from Hipotronics, Inc. (Model 803-330), operating in conjunction with the temperature controllers via an isolation transformer from Abbott Company (Model S898). The unit is capable of heating substrates to temperatures up to 1000°C.

The thin-film gold–tin samples are prepared by the two-film method introduced by Shiojiri (*35, 36*). Several thousand angstroms of gold are vacuum deposited onto lacey carbon films mounted on 3-mm-diam molybdenum electron microscope grids. Tin films with an average thickness of approximately 200 Å are created by evaporation of tin (Balzers, 99.9995% purity) at rates of 15–30 Å/sec onto air-cleaved KBr substrates. The tin films are wet-stripped and collected onto the holey gold grids. This combination of the gold and tin films forms a solid–solid interface through which interdiffusion of gold and tin can take place and allows for compositional and structural changes to be observed in the electron microscope. A typical arrangement, shown in Fig. 2, consists of a thin film of tin forming a bridge over a hole bordered by the thick gold film.

The JEOL JEM-100B and JEM-200CX and the Philips EM400T and EM400ST/FEG microscopes were used in the investigation of the gold–tin thin-film system. Typical electron microscopy techniques used in the study of the thin-film gold–tin system include electron diffraction, high-resolution imaging, and energy dispersive X-ray spectroscopy. The electron beam was also used as a source of heat in the *in situ* heating experiments.

X-ray collection conditions were varied depending on the microscope used. Typical conditions on the Philips EM400T were 100–500 Å diameter probe size, 120 kV accelerating voltage, 300 sec counting time, and 30° specimen tilt. Spectra were collected with a room-temperature specimen holder. Conditions typically used on the Philips EM400ST/FEG microscope were 50–100 Å probe size, 100 kV accelerating voltage, 50–300 sec counting time, and 10° specimen tilt. Most of the spectra were collected using a liquid nitrogen-cooled specimen stage.

The standardization of the peak ratios were performed on the Philips EM400ST/FEG using a liquid nitrogen stage. Crushed AuSn, $AuSn_2$, and $AuSn_4$ alloys of known compositions were prepared and analyzed. The bulk alloy crystals were verified by electron diffraction patterns matching the respective calculated patterns. A total of 37 spectra taken from the crystals of the three bulk phases were used to compute the value of k_{Au-Sn} in the Cliff-Lorimer relationship, which is expressed in the following form:

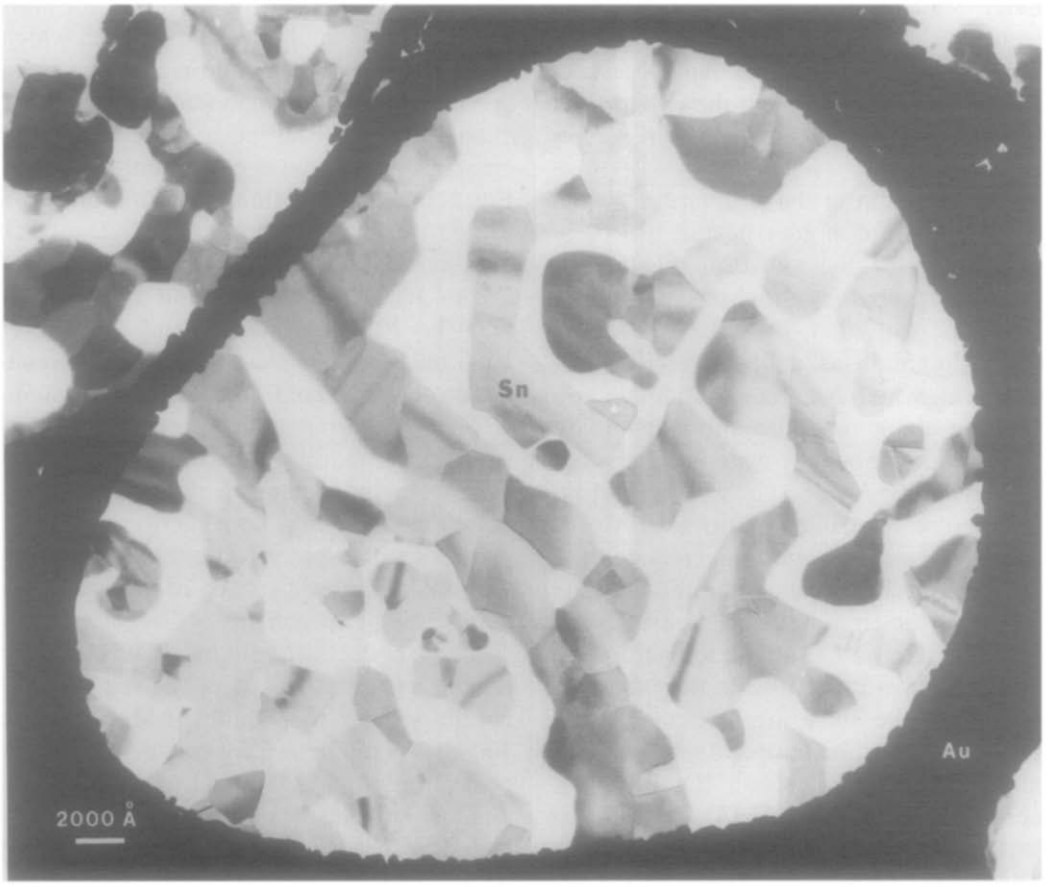

FIG. 2. A typical arrangement of gold and tin films. The tin films consist of ribbons of interconnected grains and islands of 2000–5000 Å in diameter and supported on a carbonaceous layer over the holes in the thicker gold films.

$$\frac{C_{Au}}{C_{Sn}} = k_{Au\text{-}Sn} \frac{I_{Au}}{I_{Sn}}.$$

The calculated value of $k_{Au\text{-}Sn}$, expressed within a 95% confidence level, is 1.9 ± 0.1.

To determine the significance of compositional changes within a given sampling area, the following precision measurements were performed. Two regions from a gold–tin thin-film alloy were chosen for analysis on the Philips EM400ST/FEG. Ten consecutive spectra were collected from each region, and the compositions were calculated. The precision of the composition measurements, at the 95% confidence level, was ± 0.1, i.e., $AuSn_{1.0\pm0.1}$. Thus, changes in composition greater than this precision limit would be considered significant.

Results

The Effect of Preheating the Two-Film System

In the two-film arrangement, interdiffusion of gold and tin did not occur immediately after contact was made between the two films. Different heating methods were used on the gold–tin couples to initiate the reactions. In most cases, the grids were

FIG. 3. A two-film arrangement of gold and tin films showing the effects of heating at 200°C for 10 min. The grayish areas represent amorphous layers left behind by the recession of the tin films.

heated in evacuated glass tubes at 200°C for 10 min.

One of the most obvious effects of heating is shown in Fig. 3. Here, transport of tin within some grains of the tin films took place, which left behind an amorphous layer. The edges of these amorphous layers delineated the shapes of the original tin

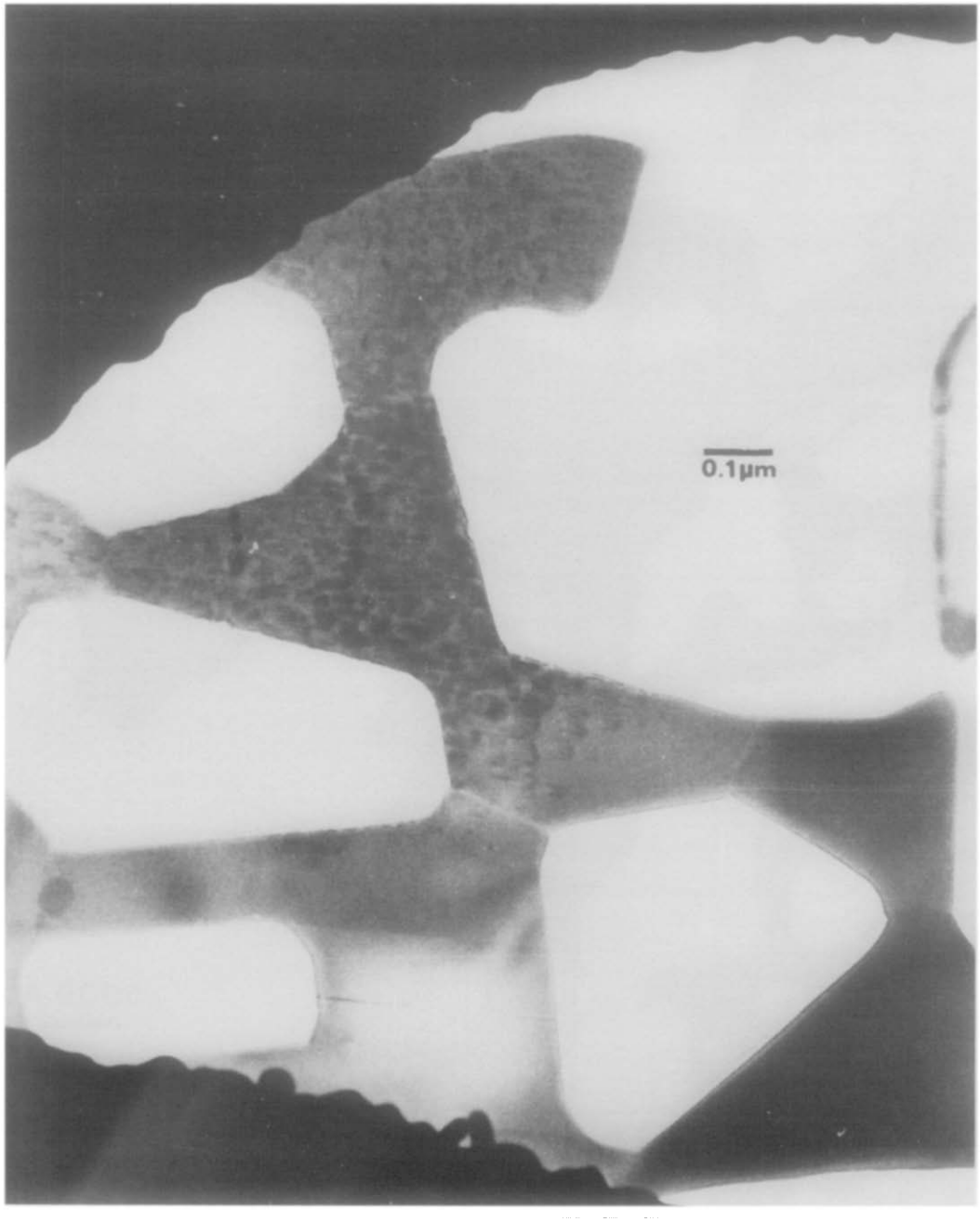

FIG. 4. An image of a tin film showing signs of reaction with gold after heating at 200°C for 10 min. The morphology of the reacted films is different from the unreacted films in Fig. 2.

films. Furthermore, the amorphous layers replicate the locations of the original grain boundaries. An EELS spectrum showing a very strong carbon K peak (280 eV) and a very weak tin $M_{4,5}$ peak (510 eV) established the presence of carbon and a little tin in these layers.

Other effects of heating at 200°C are

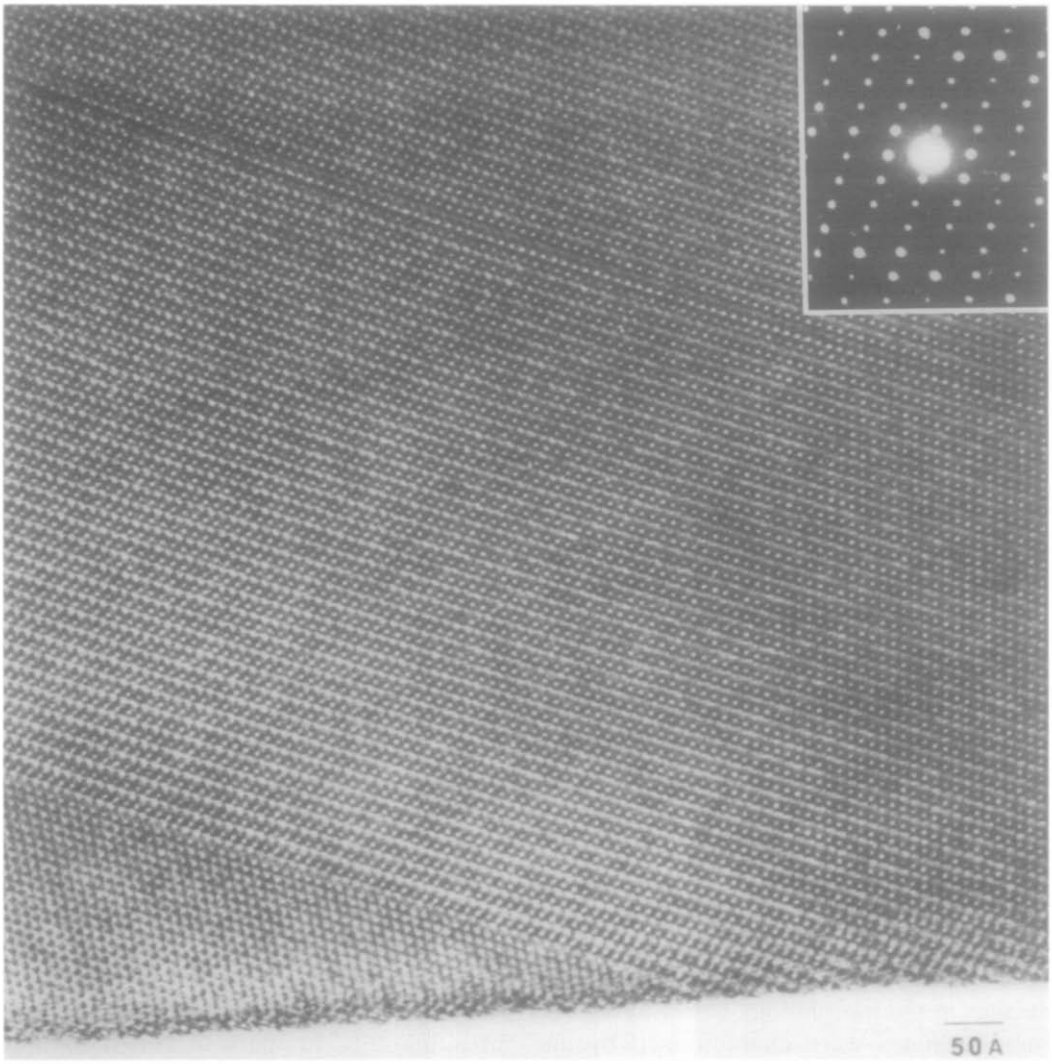

FIG. 5. A high-resolution image of a region of the reacted film in Fig. 4. The upper region of the image consists of 8 × 13-Å blocks, as indicated by the accompanying diffraction pattern. In the bottom portion, a region of a hexagonal-like array of 7-Å fringes is defined by a sharp boundary.

shown in Fig. 4. The morphology of the tin film was markedly different from that of the unreacted β-tin films. In this figure, the appearance of mottling and striations as well as the general darkening and thinning of the individual grains represented signs of apparent reaction. A high-resolution image taken from the reacted film in Fig. 4 is shown in Fig. 5. The image, unidentified for reasons to be discussed later, consists largely of a periodic array of 8 × 13-Å blocks, as indicated by the accompanying diffraction pattern. In the lower quadrant of the image, a coherent boundary separates the upper region from a region consisting of a hexagonal-like array of fringes of about 7 Å. This is an unknown Au–Sn phase believed to have a composition $AuSn_2$ (and

hereafter designated $AuSn_2$ (ms) from experiments to be described later. Although unidentified on the basis of comparisons with models of known phases, this image is included as an example of the numerous observations of unknown Au–Sn phases.

As a check to determine whether the crystalline phases observed in Figs. 4 and 5 were indeed the result of the reaction with gold or of a polymorphic transformation in β-tin, grids containing β-tin films mounted on plain holey carbon films with no gold were heated *in vacuo* (10^{-3} Torr) at 200°C for 10 min. Electron microscopy of these films revealed no polymorphism or phases having diffraction patterns similar to the one in Fig. 5. Instead, lattice spot patterns representing the [100] and [001] zones of β-tin and a [212] zone of SnO_2 were found.

The Effect of Beam Heating Single-Film Diffusion Arrangements

An example of the effect of electron beam heating of the films in the electron microscope is shown in Fig. 6. The tin film was mounted on a plain holey carbon grid, and gold was deposited in the form of 25 to 50-Å islands about 5 months later. The electron beam was condensed on the specimen for a period of 5 min when noticeable changes in the morphology began to occur. These changes were characterized by an apparent thickening and thinning of the films as well as a loss of bend extinction contours in some regions as shown in the "after" picture.

A high magnification image of a region of the electron-beam heated film in Fig. 6 was taken. The evaporated gold islands were clearly visible as dark spots. A high-resolution image was also made from a small region. The diffraction pattern matched the calculated [110] zone pattern of $AuSn_4$. The image showed fringes from the (002) and ($1\bar{1}1$) planes of $AuSn_4$ (5.8 and 4.2 Å, respectively). The dark spots in the image corresponded to regions originally occupied by the gold islands.

In an *in situ* preparation, a thin film of tin was deposited at 15 Å/sec to an average of 200 Å onto KBr and followed immediately by the deposition of 50-Å gold islands without breaking the vacuum. Observations made within one hour after this preparation revealed immediate reactions in the tin films, confirming earlier reports of rapid interdiffusion. Electron diffraction patterns from the various grains in the reacted films revealed the presence of $AuSn_4$ and $AuSn_2$ on the basis of comparison with the calculated diffraction patterns of the known Au–Sn phases.

In situ Heating of the Two-Film Configuration

A series of heating experiments was performed on the KRATOS EM1500 1.5-MeV high-voltage electron microscope (HVEM) located at the National Center for High Voltage Electron Microscopy, Lawrence Berkeley Laboratory, Berkeley, California. It is equipped with a double-tilt, side-entry heating specimen stage, allowing the user to observe heating effects up to about 800°C.

A freshly prepared grid sample containing a tin film on a holey gold film was observed on the 1.5 MeV HVEM. Two pictures, taken 1.5 hr apart, of a [100] oriented β-tin film over a hole are shown in Fig. 7. The image at the left shows the film taken at 196°C, while the other was taken at 256°C. The observed effect was the disappearance of a grain of presumably β-tin at the lower left-hand portion of the hole at temperatures around the melting point of tin (231°C). Other films, presumably β-tin in the surrounding holes also exhibited evidence of changes.

Another thin-film region was imaged in two sequential photographs in Fig. 8 taken 15 min apart, with the photograph at the left taken at 350°C. The large grain in the right

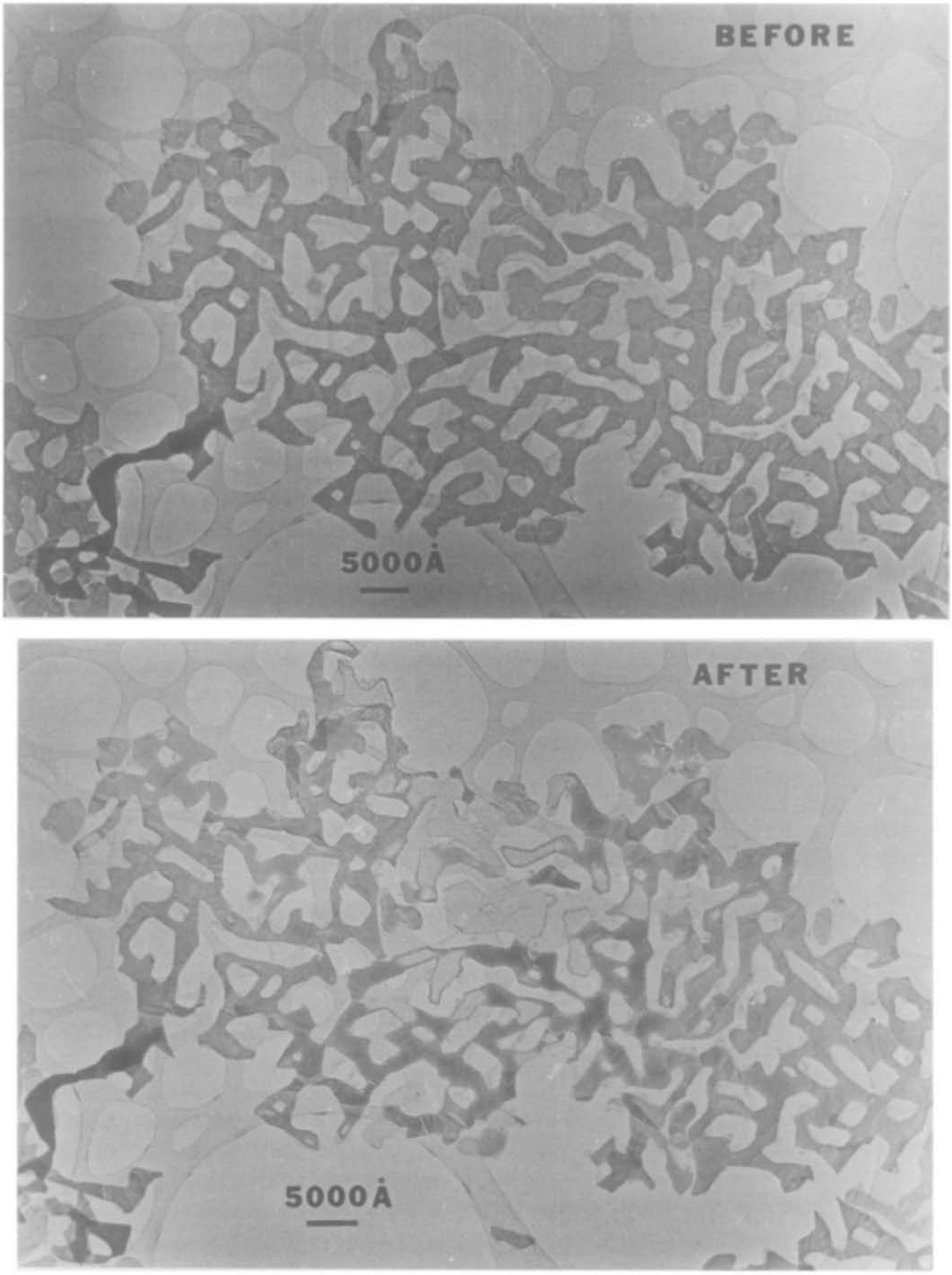

FIG. 6. An example of electron-beam heating of thin films. The tin films support evaporated gold islands 25–30 Å in diameter. Condensing the electron beam for 15 min results in changes similar to those in Fig. 3.

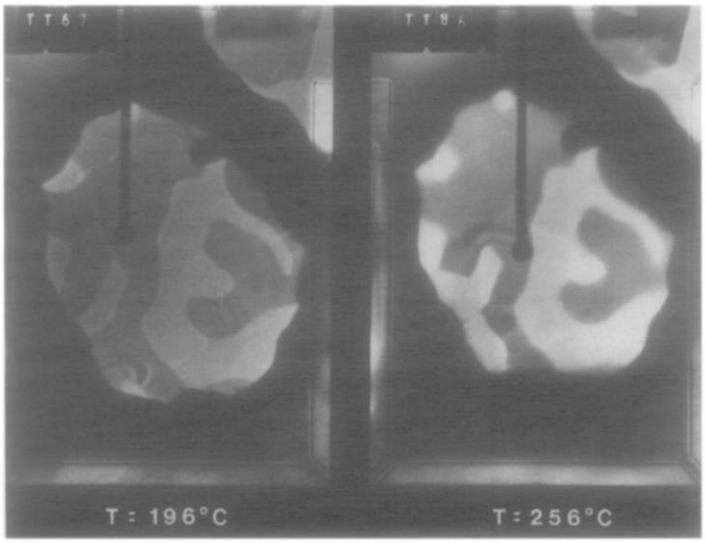

FIG. 7. Thin films of tin during heating in the KRATOS EM1500 at 196 and 256°C. Note the disappearance of the grain of tin in the lower left portion of the hole in the $T = 256$°C image.

side of the hole melted at 380°C, as it became smaller and smaller and finally disappeared. The disappearance of the melted tin grain probably took place by wetting the gold layer during a 10-sec interval. The end result was the leaving of an amorphous layer shown in the photograph at the right. At 380°C, many of the films maintained their morphological integrity, while others suffered changes. A temperature of 380°C corresponds to the melting point of the ζ-phase alloy. The diffraction pattern taken from the grain in Fig. 8 was identified as [011] zone of the ζ phase. The gold-rich compositions obtained from the same crystals on the Philips EM400ST-FEG from X-

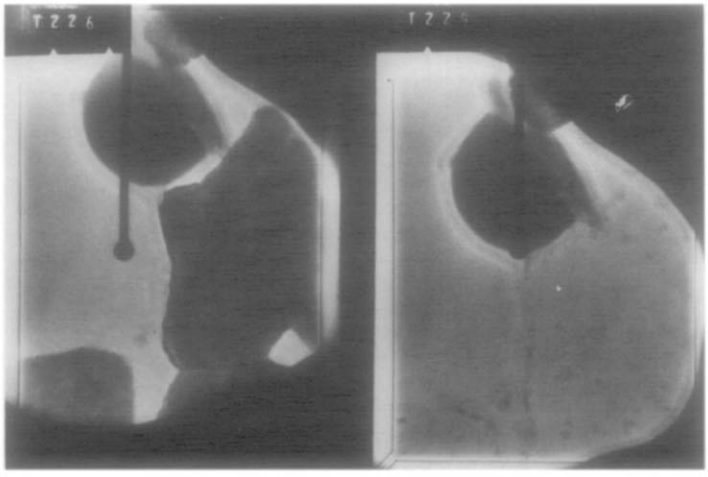

FIG. 8. Sequential photographs showing the disappearance of a ζ-phase grain at 380°C in the KRATOS EM1500. The image at the left was taken at 350°C.

FIG. 9. An image of a thin alloy film with the numbered microanalysis sampling regions. Mottling of the film surfaces and the contamination layer is the result of the electron-beam-induced formation of SnO_2 particles.

ray microanalysis results confirmed the presence of the ζ phase.

Long-Term Annealings of Two-Film Systems

An experiment was made to determine whether 200°C anneals of longer than 10 min would promote further advancement of the gold–tin reactions. Three similar holey gold grids with tin films were placed in separate sealed evacuated glass tubes and heated in a tube furnace at 200–220°C for a period of 9, 20, and 65 days, respectively. The films exhibited many of the changes already described as well as the formation of a number of isolated irregularly shaped islands (or grains) supported on the amorphous layers. The diffraction patterns from the regions in contact with the gold were identified as the [011], [211], and [001] zones of the ζ phase. Hence, gold-rich compositions were obtained in this long-term heat treatment. All realizable phase changes progressing from the tin-rich side of the phase diagram already would have occurred before the formation of these ζ phases. The 20- and 65-day treatments produced the same results.

X-ray Microanalysis of Au–Sn Alloys

In the image of an alloy film in Fig. 9, the numbered regions represent X-ray micro-

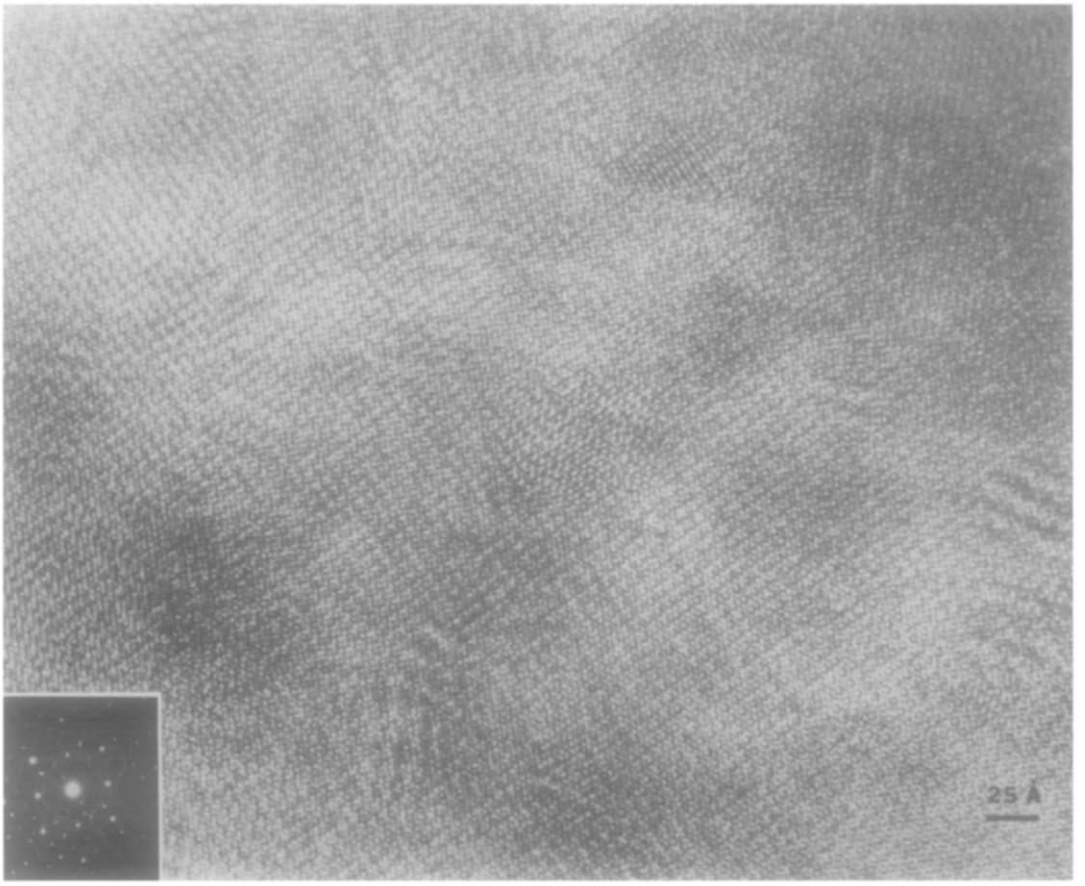

FIG. 10. A high-resolution image of a region of the alloy film in Fig. 9. The formation of SnO_2 is indicated by the Debye rings in the diffraction pattern. The image of the alloy having a composition of $AuSn_2$ consists of 6 × 6-Å fringes with extensive finer contrast with some moiré fringes probably caused by overlapping SnO_2 particles.

analysis sampling areas. The X-ray collections from the crystal were done about 10 and 17 months after the preparation of the grid, at which time it was heated for 10 min at 200°C. The microanalysis results, listed in Table II, indicate a nominal composition of $AuSn_2$ in the film. Note that this particular microanalysis experiment was done after the apparent surface oxidation had already occurred. Therefore, the intensity of the tin peaks represents the total amount of tin present in the sample, namely, the tin in both the alloy and the SnO_2. Since the distribution of tin was unknown, the listed compositions of the alloy in Table II would be the upper limit values.

A high-resolution image of the crystal in Fig. 9 is shown in Fig. 10. The array of strong spots in the accompanying diffraction pattern matched the computer-calculated [101] zone of β-tin, but the rest of the pattern could not be identified on the basis of known Au–Sn phases.

A series of experiments was performed on a freshly prepared grid sample that had been heat-treated *in vacuo* at 200°C for 10 min prior to the microscope session. The purpose of this experiment was to perform

TABLE II

X-RAY MICROANALYSIS RESULTS TAKEN FROM THE GOLD–TIN THIN-FILM IN FIG. 9[a]

Region	Composition	
	First collection	7 months later
1	$AuSn_{2.0}$	$AuSn_{1.9}$
2	Hole count	
3	$AuSn_{2.0}$	$AuSn_{1.9}$
4	$AuSn_{1.6}$[b]	$AuSn_{1.5}$
5	$AuSn_{1.8}$	$AuSn_{1.5}$
6	$AuSn_{2.2}$	$AuSn_{2.3}$

[a] Collection conditions: Accelerating voltage, 100 kV; Probe size, ~50 Å; Collection time, 300 sec; Sample tilt, $x = 10°$, $y = 0°$; Sample temperature, −184°C.

[b] High gold count due to specimen drift with the probe moving toward the holey gold edge during the x-ray collection.

X-ray microanalysis on the gold–tin films without the formation of SnO_2. The liquid nitrogen specimen stage of the Philips EM400ST/FEG was used in these experiments to minimize oxidation and contamination buildup. The alloy film is shown in Fig. 11. X-ray collections were performed during the first 4 days, on the 50th, and on the 130th day. The compositions of the film are listed in Table III.

A number of diffraction patterns were taken from various regions of the crystal in Fig. 11. The diffraction patterns from regions 7, 9, and 10 were identified as the [011] zone of AuSn, in agreement with the AuSn compositions of those regions. The AuSn composition was consistently the same for those regions during the entire experiment.

In the remaining regions, the nominal composition was $AuSn_2$. The diffraction patterns from regions 1, 3, 6, 8, and 11, however, were not representative of the bulk $AuSn_2$ diffraction patterns. These diffraction patterns remained unchanged through the first 50 days. Between 50 and 130 days, a composition change occurred, as indicated by the increasing gold content in the $AuSn_2$ (ms) regions. A diffraction pattern taken from regions 3 and 6 after 130 days showed strong spots from the [011] zone of AuSn, along with a separate very weak pattern, unchanged from the beginning. The location of the nominal composi-

TABLE III

X-RAY MICROANALYSIS RESULTS FROM THE GOLD–TIN CRYSTAL IN FIG. 11[a]

Region	Composition (by days)					
	1	2	3	4[b]	50	130
1	$AuSn_{2.3}$	$AuSn_{2.0}$	$AuSn_{1.8}$	$AuSn_{2.1}$	$AuSn_{2.5}$	$AuSn_{1.6}$
2			(Hole count)			
3	$AuSn_{2.2}$	$AuSn_{1.9}$	—	$AuSn_{2.4}$	$AuSn_{2.2}$	$AuSn_{1.3}$
4	$AuSn_{2.2}$	$AuSn_{2.2}$	—	$AuSn_{2.3}$	$AuSn_{2.6}$	$AuSn_{1.4}$
5	$AuSn_{2.5}$	$AuSn_{2.2}$	—	$AuSn_{2.3}$	$AuSn_{2.8}$	$AuSn_{2.0}$
6	$AuSn_{2.1}$	$AuSn_{2.0}$	—	$AuSn_{2.3}$	$AuSn_{2.3}$	$AuSn_{1.1}$
7	AuSn	$Au_{1.1}Sn$	AuSn	$AuSn_{1.3}$	$AuSn_{1.9}$	$Au_{1.1}Sn$
8	$AuSn_{2.3}$	$AuSn_{2.0}$	—	$AuSn_{2.6}$	—	$AuSn_{2.0}$
9	AuSn	$AuSn_{1.1}$	—	—	—	AuSn
10	$AuSn_{1.2}$	$AuSn_{1.3}$	—	—	—	$Au_{1.1}Sn$
11	$AuSn_{2.0}$	$AuSn_{2.0}$	—	—	—	$AuSn_{1.5}$

[a] Experimental conditions: 300-sec counts; ~50- to 100-Å probe size; Tilt, $x = 10°$, $y = 0°$; $T = -184°C$.

[b] Data taken at $T = 22°C$.

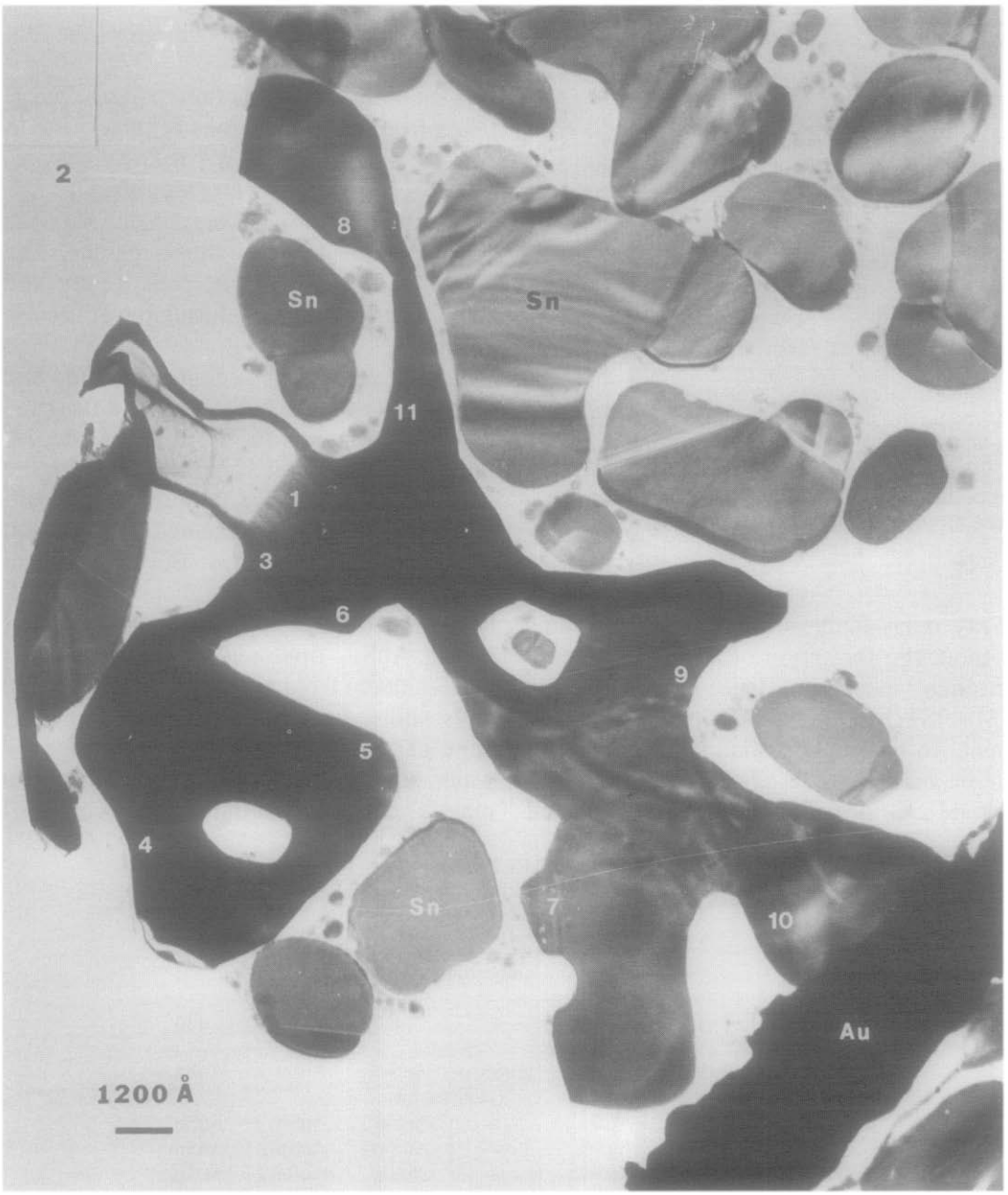

FIG. 11. An image of a thin alloy film with the microanalysis sampling regions marked. Regions 7, 9, and 10 have the AuSn composition. The remaining regions have a nominal composition of $AuSn_2$. The tin islands are suspended over the hole by an amorphous contamination layer.

tion of $AuSn_{1.5}$ in the gold–tin phase diagram would be in the two-phase region between AuSn and $AuSn_2$ (ms) in agreement with observation.

Other Unidentified Structures

The identification of the gold–tin phases was done by analysis of the selected area

TABLE IV

ELECTRON DIFFRACTION ZONES OF IDENTIFIED PHASES

Phase	Diffraction zones found
Sn	[100],[001],[110],[101],[133]
$AuSn_4$	[100],[001],[110],[102],[121],[221]*,[112]*
$AuSn_2$	[011],[111],[201],[120],[112]*,[211]*
AuSn	[101],[102],[210],[121],[122]
Zeta	[001],[101],[211]
SnO_2	Powder rings, [100]*,[101]*,[001],[212]
Au	Powder rings

* Not positively identified, but it is a best possible match with the calculated zones.

electron diffraction patterns obtained. These patterns were compared with those computed by the DIFPLT program, written by Skarnulis (*37*), on the IBM 360/370 computer. The calculation is based on kinematical, single-scattering intensities.

Hundreds of diffraction patterns obtained in this work were measured and grouped into types classified on the basis of the diffraction zones of the known phases and the geometries of the unidentified phases. Of over 60 different types of diffraction patterns, 33 were identified on the basis of the known parameters of the bulk phases. Table IV lists the identified diffraction zones of the phases present in the thin films. The zones denoted by asterisks were those not positively identified, but were the best possible matches with the DIFPLT-calculated zones.

The remaining unidentified diffraction patterns were found to have geometrical arrangements of diffracted spots different from those of the calculated patterns of the known phases. The most striking aspect of these patterns was the presence of measured d spacings larger than those of the bulk gold–tin phases. The diffraction patterns accompanying the images in Figs. 5 and 10 were some of the representative examples of the unidentified patterns typically found in the thin-film reactions.

A surprising observation was noted in the microanalysis studies of the gold–tin films using the liquid nitrogen specimen stage. There were no indications of the β-to-α transition in the tin films. The specimen temperature of -180°C was well below the 18°C transition temperature, but no transformations were observed.

Discussion

The Causes of Delayed Chemical Reaction

The lack of interdiffusion of gold and tin immediately after contact between the two films was made was unexpected in view of the several diffusion studies (*21, 29, 31, 32*). To induce the reactions in most of the gold–tin couples, heating is necessary. This failure to obtain immediate reactions at room temperature suggests the presence of a barrier between the gold and tin films which is eventually overcome by heating.

There are many possible causes for this initial lack of reaction. The most effective would be very poor contact between the films. This could result from the roughness and nonuniformity of the film surfaces or buckling of the tin films due to temperature changes that may actually promote varying degrees of contact. This was observed in many of the heated grid samples, where reacted films were found among unreacted ones on the same grid. In regions of limited contact between the films, the diffusion of gold into tin may be restricted by this "bottleneck" effect. Obviously, good contact between the gold and tin films is a requirement for the prompt initiation and maintenance of the reactions.

Another possible cause of the lack of reaction in the gold–tin couples is the presence of surface oxides. The presence of a surface oxide, SnO_2, has been reported by Buene (*21*) to be a barrier for the diffusion process. However, in these experiments, oxide formation on the fresh films was not

observed and, unless there was an amorphous oxide layer, this does not appear to have been the chief deterrent to reaction. This suggests that a contamination layer may be the principal shield protecting the β-tin films from oxidation in most cases. The observed oxidation of the clusters of tin trapped in the amorphous matrix appears to be electron beam-induced oxidation by residual oxygen in the system, not by the exposure of the tin films to air. A contamination layer would minimize the oxidation of the β-tin films upon removal from the vacuum system.

The tin film in Fig. 3 shows the presence of an amorphous contamination layer along the edges. The layers are further revealed by the heating experiments in which tin was transported exposing an amorphous support. This strongly suggests that they were formed by the condensation of the residual vapors on the substrate surfaces before the actual tin depositions and were wet-stripped with the tin. The vacuum system requires a pumpdown time of about 2 hr to reach the 10^{-7}-Torr pressure range, which is enough time to allow for this condensation. The impinging tin atoms may not actually come into contact with the KBr surfaces. Thus, the condensed carbonaceous layers could also provide a nucleation barrier that might modify the growth of the tin films.

Another unusual behavior, possibly effected by the amorphous layers, is the lack of the observed β-to-α transitions in the tin films at low temperatures. α-Tin has a diamond-cubic structure with a volume greater by 20% than that of β-tin. With this large volume difference, the formation of the α phase within β is difficult, unless suitable embryos of the α phase can be nucleated on the surfaces of β-tin. Smith and Raynor (*38*) have found that if surface oxides are present, the transformation will not take place. Crystalline oxides of tin were not found in the films cooled far below the transition temperature in the liquid nitrogen stage, suggesting the presence of protective amorphous contamination layers such as have been demonstrated.

Diffusion of gold through the contamination layer does take place during the 10-min 200°C heating process. Ackermann, Vermaak, and Snyman (*39*) have studied the effects of amorphous carbon films of different thicknesses in the reactions of evaporated copper films on solution-grown gold microcrystals. With carbon layers up to 50 Å thick, direct interaction between the overgrowth and substrate leading to the formation of both continuous and ordered solid solutions has been confirmed by selected-area diffraction patterns. For the carbon layers with thicknesses greater than 70 Å, the resulting copper overgrowth was found to be completely polycrystalline, with no indication of the formation of any of the gold–copper solid solutions. These observations are consistent with the work being discussed here. Diffusion through the contamination layer is very slow at room temperature, but it is accelerated at higher temperatures.

The deposition of gold islands directly onto the thin films of tin, have resulted in the formation of stoichiometric tin-rich alloys. The deposition of the gold islands insures that the concentration of gold is less than that of tin in the film. The *in situ* depositions have produced the $AuSn_2$ and $AuSn_4$ phases in the films, as described before. In these depositions, the gold islands were evaporated onto the tin films within 5 min of the deposition of the tin. Contamination buildup should be slight during this time period. The immediate growth of the $AuSn_2$ and $AuSn_4$ phases occurs. The result is the same when the $AuSn_4$ phase was formed by electron-beam heating of a 5-month old tin film on which gold islands were deposited. Heating was necessary, in this case, in order to induce diffusion of gold from the islands through the contamination layer on the tin films.

The two-film method as used here is very

effective in controlling the rate and extent of the gold–tin reactions. The compositions of the films are controlled by the thickness of the amorphous layers, the length of the heating times and the amount of tin available to react with the incoming gold atoms.

It was expected that the formation of the gold–tin phases would proceed from the tin-rich side of the phase diagram and continue toward the gold-rich side since gold is the diffusing species. In this case, the thin-film configuration would result in the formation of a "miniature" phase diagram, which permits the formation of the gold–tin phases to be observed as a progressive series of interfaces with the gold-rich phases being contiguous with the gold source. However, this progressive series of interfaces was never observed in any of the films studied. Instead, many of the interfaces were limited to the grain boundaries in the tin films.

Structural Relationships and Metastable Products

There are a number of considerations in the identification of the many unknown gold–tin phases found in this work. The high-resolution image in Fig. 5 is still not explained. Assuming the diffraction pattern to be that of a [011] zone of a hexagonal unit cell, and assigning the measured values 13 and 8 Å as d spacings for the (100) and (01$\bar{1}$) planes, respectively, the calculation of the new lattice parameters results in a hexagonal unit cell having $a = 15$ Å and $c = 11$ Å. A superstructure of one of the gold–tin phases having these dimensions would be possible. The regular enhancement of some of the spots of the diffraction pattern is responsible for the subcell contrast. The hexagonal AuSn unit cell could be realized by the transformation matrix 2$\bar{2}$0/240/002. The composition could be varied in the same manner as for the NiAs structure described earlier by removing gold atoms to obtain the tin-rich compositions. However, calculations on the image comparator, described by Rae-Smith and Eyring (*40*), produced images that could not be satisfactorily compared with those in Fig. 5. Hence, although the unit cell can be rationalized, guessing the true structure is very difficult.

The gold–tin alloy film in Fig. 11 shows a distinct two-phase separation, as indicated by the microanalysis results. The more gold-rich phase, AuSn, is located nearer the source of the gold atoms than the less gold-rich phase of composition $AuSn_2$ (ms). The AuSn composition remained constant while the composition of the region occupied by the unknown $AuSn_2$ (ms) phase changed slowly to $AuSn_{1.5}$. This final composition suggests a two-phase mixture of AuSn and $AuSn_2$ (ms) in agreement with a diffraction pattern taken on the 130th day that shows the strong spots of [011] AuSn with an overlay of very weak spots from the original $AuSn_2$ (ms) phase. This shift of intensities suggests the formation of the AuSn phase at the expense of the $AuSn_2$ (ms) phase. A possible reaction sequence would begin with the conversion of the entire film into the *gold-deficient* Au–Sn alloy having the NiAs structure, with the gold-poor regions being the metastable $AuSn_2$ phase. Restricted diffusion of gold through the AuSn phase then saturates part of the metastable region, leading to partial conversion of the metastable phase into AuSn. This takes place by the filling of the gold-deficient AuSn structure by the diffusing gold atoms to achieve the stoichiometric AuSn structure. Kjekshus and Pearson (*41*) have written a comprehensive review of the NiAs structures in which different structural arrangements, leading to compositional variations, have been described.

In the interpretation of the diffraction pattern of Fig. 10, the subcell has been determined to be beta-tin in the [101] orientation. Using the β-tin unit cell as a model,

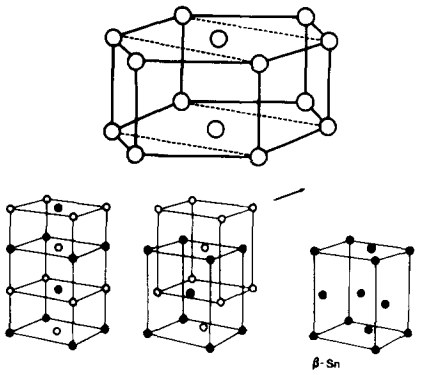

FIG. 12. The derivation of the β-tin structure from a h.c.p. structure utilizing the orthohexagonal representation.

the unit cell vectors of β-tin have been transformed into new vectors by the matrix $101/\frac{1}{2}\,\frac{1}{2}\,-\frac{3}{2}/011$. This transformation results in a triclinic unit cell with the parameters $a = 6.6$ Å, $b = 6.3$ Å, $c = 6.6$ Å, $\alpha = 87.5°$, $\beta = 76.7°$, $\gamma = 87.5°$. The length of the lattice vector along the electron beam direction ([101]) is not confirmed because of a lack of an available diffraction pattern in a different zonal orientation. The length of the *a*-axis vector would be some multiple of the [100] projection of 6.6 Å. The transformed unit cell consists of four equally spaced layers of tin atoms, with each layer containing four tin atoms. This arrangement is very similar to the layered structure of tin atoms in the $AuSn_4$ unit cell. The new phase would then form by diffusion of gold atoms into the β-tin structure in such a way that ordering in the transformed unit cell is produced. Again, as in the previous case, the positions of the gold and tin atoms in the new transformed cell are not known. In both cases, the computer-calculated diffraction patterns for the transformed unit cells matches the experimental diffraction patterns perfectly. In neither were satisfactory image matches obtained.

The diffraction pattern, shown in Fig. 10, showing the strong spots of [101] β-tin offers another possible interpretation. The enhancement of the subcell spots can be due to the formation of the "stuffed" β-tin structures described by Parthé (*42*). The framework of these compounds consists of a skeleton similar to the β-tin structure, which has the unique property of permitting the insertion of filler atoms in a regular fashion. The filler atoms are inserted into the framework as equally spaced pairs, with each pair rotated with respect to the neighboring pair. The symmetry of the β-tin subcell is essentially unchanged by the filling process, thus resulting in the formation of superstructures. It is possible that the diffraction pattern in Fig. 10 represents a superstructure of beta-tin filled with enough gold atoms to achieve the $AuSn_2$ composition.

Buene *et al.* (*25*) have illustrated, in structural terms, how $AuSn_4$ can be nucleated in the β-tin structure without it being significantly changed. However, how the AuSn phase can be nucleated in β-tin as a first-formed phase was not discussed. Two ways of seeing the relationships are suggested as follows.

Since the AuSn structure consists of an h.c.p. array of tin atoms with gold atoms in the octahedral holes, the nucleation of AuSn in the β-tin matrix can be facilitated in terms of an orthohexagonal relationship described by Kane, Giessen, and Grant (*43*) and Raynor and Lee (*44*). This relationship is illustrated in Fig. 12. Consider an end-centered orthorhombic unit cell to be derived from a simple hexagonal structure. By stacking three of these end-centered orthorhombic cells as shown, a structure, containing two interpenetrating body-centered orthorhombic subcells, is obtained. By shifting one of the body-centered orthorhombic subcells by one-fourth of one of the lattice directions with respect to the other, the β-tin unit cell is obtained. Thus the β-tin unit cell is related to a simple hexagonal unit cell by shifting the atoms at $(\frac{1}{2}, 0, \frac{1}{4})$ and $(0, \frac{1}{2}, \frac{3}{4})$ by $\pm$ c/4.

The second model is more subtle. The

arrangement of the tin atoms in the AuSn structure, viewed in the [001] projection, is very similar to the arrangement of the β-tin atoms in the [$\bar{1}$03] projection of the β-tin unit cell. The [$\bar{1}$03] direction is nearly perpendicular to the ($\bar{1}$01) planes of β-tin, which have a d spacing of 2.7 Å. Doubling the value of this d spacing yields the value of 5.4 Å, which is close to the AuSn c-axis length of 5.5 Å. The a, b, and c axes of the β-tin unit cell are transformed to directions parallel to [111], [$\bar{1}$11], and [$\bar{1}$03] of β-tin, respectively. This results in a transformed β-tin unit cell with the parameters, $a = b =$ 4.4 Å, $c = 5.6$ Å, $\alpha = \beta = 92.1°$, and $\gamma =$ 82.6°. With the exception of the value of γ, the parameters are nearly the same as those of the AuSn unit cell. Thus, it is possible for AuSn to nucleate in a β-tin matrix without gross reconstruction.

The reactions observed here have taken place at temperatures slightly higher than the lowest temperature on the gold–tin phase diagram (127°C, Fig. 1) or at room temperature. Therefore, the unknown phases could be low-temperature ordered phases that decompose at higher temperature. Alternatively, they could be explained as kinetically stranded metastable structures. According to Buene *et al.* (*25*), the AuSn and $AuSn_4$ phases are formed first, and $AuSn_2$ results from a subsequent transformation of the AuSn phase. This suggests that the free energy difference for the nucleation of the bulk $AuSn_2$ in a β-tin matrix is large compared to that of the AuSn and $AuSn_4$, because of the structural similarities and the relative ease of the transformation of β-tin into $AuSn_4$ or AuSn. Thus, the lack of any structural relationship between β-tin and $AuSn_2$ accounts for the difficulty of the $AuSn_2$ phase to nucleate as a first-formed phase. It is frequently found (Christian (*45*)) that a metastable precipitate forms more rapidly than the equilibrium precipitate when it is coherent with the parent matrix while the equilibrium precipitate is not. Thus, in this case, the unknown $AuSn_2$ (ms) phase is probably metastable with a structure that is coherent with the matrix structure of β-tin. The diffusion barrier between the gold and tin films controls the amount of gold diffusing into tin in an amount to form a composition of $AuSn_2$ in the film.

Conclusions

The HREM observations have revealed many reactions in the thin films, most of which were brought about by some form of heating. The initial lack of reaction in the thin-film couples has been determined to be due to the presence of an amorphous carbonaceous layer. This layer is the result of the condensation of residual vapors in the vacuum system onto the KBr substrates prior to the tin depositions. During the wet-stripping process, it is removed from the substrate surfaces along with the tin films to form an intervening layer between the gold and tin films in the two-film arrangement. The contamination layers could also protect the tin films from oxidation due to exposure to air. It has been determined that the diffusion barrier, imposed by the contamination layers, can be overcome by heating, typically at 200°C, eventually resulting in the observation of several known and previously unknown structures. When gold islands are deposited on tin films the rate of reaction depends upon the degree of contamination of the tin film before the gold is evaporated. Several possibilities for the formation of the new phases have been described in terms of structural models and kinetic arguments. The rate of formation and extent of the gold–tin reactions can be effectively controlled by adjusting the contamination layer. This thin-film arrangement alters the reaction sequence of the gold–tin reactions in a way not observed in standard, bulk-prepared specimens. Thus, the formation of new possibly metastable gold–tin phases in the thin films is facilitated by the presence of impurities in the form of amorphous contamination layers.

Acknowledgments

It is a pleasure to acknowledge the efforts of Michael McKelvy and Lane Briley in the construction of the evaporator system and of K. H. Westmacott for making the KRATOS EM1500 available for high-temperature observations. R. W. Carpenter generously provided instruction in the use of the Philips EM400ST/FEG microscope. The financial support for this research, provided by the National Science Foundation Grant DMR-8108306, and the use of the Facility for High Resolution Electron Microscopy at Arizona State University, supported by the National Science Foundation Grant DMR-8306501, are gratefully acknowledged.

References

1. R. VOGEL, *Z. Anorg. Chem.* **46,** 60 (1905).
2. H. E. SWANSON AND E. TATGE, *NBS Circ.* **539,** 24 (1953).
3. H. E. SWANSON AND E. TATGE, *NBS Circ.* **539,** 33 (1953).
4. K. SCHUBERT, H. BREIMER, AND R. GÖHLE, *Z. Metallkd.* **50,** 146 (1959).
5. B. HENDERSON AND G. V. RAYNOR, *Trans. Faraday Soc.* **58,** 900 (1962).
6. T. B. MASSALSKI AND H. W. KING, *Acta Metall.* **8,** 677 (1960).
7. B. HENDERSON AND G. V. RAYNOR, *Proc. R. Soc. London Ser. A* **267,** 313 (1962).
8. B. C. GIESSEN, *Z. Metallkd.* **59,** 805 (1968).
9. K. OSADA, S. YAMAGUCHI, AND M. HIRABAYASHI, *Trans. Jpn. Inst. Met.* **15,** 256 (1974).
10. W. B. PEARSON, "A Handbook of Lattice Spacings and Structures of Metals and Alloys," Vol. 2, p. 681. Pergamon, New York, 1966.
11. G. D. PRESTON AND E. A. OWEN, *Philos. Mag.* **4,** 133 (1927).
12. S. STENBECK AND A. WESTGREN, *Z. Phys. Chem. B* **14,** 91 (1931).
13. J. A. BOTTEMA AND F. M. JAEGER, *Proc. R. Acad. Sci. Amsterdam* **35,** 916 (1932).
14. V. I. PSAREV, V. G. KIRIY, A. V. KUZNETSOV, I. V. PSAREVA, AND A. L. IVANOVA, *Russian Metall.,* 175 (1982).
15. J. S. CHARLTON, M. CORDEY-HAYES, AND I. R. HARRIS, *J. Less-Common Met.* **20,** 105 (1970).
16. P. I. KRIPEYAKEVICH, *Sov. Phys. Crystallogr.* **20,** 168 (1975).
17. K. SCHUBERT, U. RÖSLER, M. KLUGE, K. ANDERKO, AND L. HÄRLE, *Naturwissenschaften* **40,** 437 (1953).
18. K. SCHUBERT AND U. RÖSLER, *Z. Metallkd.* **41,** 298 (1950).
19. J.-P. JAN, W. B. PEARSON, A. KJEKSHUS, AND S. B. WOODS, *Can. J. Phys.* **41,** 2252 (1963).
20. B. F. DYSON, *J. Appl. Phys.* **37,** 2375 (1966).
21. L. BUENE, *Thin Solid Films* **43,** 285 (1977).
22. L. BUENE, *Thin Solid Films* **47,** 159 (1977).
23. L. BUENE AND S.-T. JACOBSEN, *Phys. Scr.* **18,** 397 (1978).
24. L. BUENE, H. FALKENBERG-ARELL, AND J. TAFTØ, *Thin Solid Films* **65,** 247 (1980).
25. L. BUENE, H. FALKENBERG-ARELL, J. GJØNNES, AND J. TAFTØ, *Thin Solid Films* **67,** 95 (1980).
26. D. GREGERSEN, L. BUENE, T. FINSTAD, O. LONSJO, AND T. OLSEN, *Thin Solid Films* **78,** 95 (1981).
27. B. HUGSTED, L. BUENE, T. FINSTAD, O. LONSJO, AND T. OLSEN, *Thin Solid Films* **98,** 81 (1982).
28. S. NAKAHARA AND R. J. MCCOY, *Thin Solid Films* **72,** 457 (1980).
29. S. NAKAHARA AND R. J. MCCOY, *Appl. Phys. Lett.* **37,** 42 (1980).
30. S. NAKAHARA, R. J. MCCOY, L. BUENE, AND J. M. VANDENBERG, *Thin Solid Films* **84,** 185 (1981).
31. V. SIMIĆ AND Z. MARINKOVIĆ, *J. Less-Common Met.* **51,** 177 (1977).
32. K.-N. TU AND R. ROSENBERG, Proceedings, 6th Int. Vacuum Congress 1974, *Jpn. J. Appl. Phys.* Suppl. 2, Part 1, 633 (1974).
33. G. V. RAYNOR, *in* "Symposium of the Physical Chemistry of Metallic Solutions and Intermetallic Compounds," Vol. I, pp. 312–329, Chemical Pub. Co., New York, 1960.
34. C. NABER, *Rev. Sci. Instrum.* **38,** 1161 (1967).
35. M. SHIOJIRI, C. KAITO, Y. SAITO, K. TERANISHI, AND S. SEKIMOTO, *J. Cryst. Growth* **52,** 883 (1981).
36. C. KAITO, N. NAKAMURA, K. TERANISHI, S. SEKIMOTO, AND M. SHIOJIRI, *Phys. Status Solidi A* **71,** 109 (1982).
37. A. J. SKARNULIS, Ph.D. Dissertation, Arizona State University, 1976.
38. R. W. SMITH AND G. V. RAYNOR, *Proc. Phys. Soc. B.* **70,** 1135 (1957).
39. M. ACKERMANN, J. S. VERMAAK, AND H. C. SNYMAN, *Surf. Sci.* **34,** 394 (1973).
40. A. RAE-SMITH AND L. EYRING, *Ultramicroscopy* **8,** 65 (1982).
41. A. KJEKSHUS AND W. B. PEARSON, *in* "Progress in Solid State Chemistry," Vol. I (H. Reiss, Ed.), pp. 83–174, MacMillan, New York, 1964.
42. E. PARTHÉ, *in* "Developments in the Structural Chemistry of Alloy Phases" (B. C. Giessen, Ed.), pp. 49–63, Plenum, New York, 1969.
43. R. H. KANE, B. C. GIESSEN, AND N. J. GRANT, *Acta Metall.* **14,** 605 (1966).
44. G. V. RAYNOR AND J. A. LEE, *Acta Metall.* **2,** 616 (1954).
45. J. W. CHRISTIAN, *in* "Physical Metallurgy" (R. W. Cahn, Ed.), pp. 471–587. North-Holland, Amsterdam, 1970.